Absence of Galilean invariance for pure-quartic solitons

Justin Widjaja [1], Erekle Kobakhidze [1], Tiernan R. Cartwright [1], Joshua P. Lourdesamy,[1] Antoine F. J. Runge,[1] Tristram J. Alexander,[1] and C. Martijn de Sterke [1,2,*]

[1]*Institute of Photonics and Optical Science (IPOS), School of Physics, University of Sydney, Sydney, New South Wales 2006, Australia*
[2]*University of Sydney Nano Institute (Sydney Nano), University of Sydney, Sydney, New South Wales 2006, Australia*

Optical temporal solitons, arising from self-phase modulation and negative quadratic (β_2) dispersion, are Galilean invariant, and therefore their properties do not depend on their group velocity. This is no longer true for pure-quartic soliton pulses arising from quartic (β_4) dispersion, for which a change in group velocity necessarily leads to nonzero quadratic and cubic (β_3) dispersion. Analyzing the generalized nonlinear Schrödinger equation for such dispersion relations analytically and numerically, we find that pure-quartic solitons are members of a larger family traveling at other speeds. These solitons, which appear to be stable, have a complex phase structure and have an asymmetric spectrum. Our results extend the understanding of solitons arising from high orders of dispersion.

I. INTRODUCTION

Temporal solitons are optical pulses arising from the interplay between the nonlinear and dispersive effects in a medium [1]. By balancing these effects, solitons propagate while maintaining their temporal and spectral shapes. These pulses have been used to develop numerous photonic applications including telecommunications [2,3], ultrafast lasers [4], optical buffers [5], and frequency comb generation [6,7]. Generally, only negative quadratic dispersion ($\beta_2 < 0$) is considered, as higher dispersion orders are usually weak and act as perturbations [8–11].

These pulses are solutions to the nonlinear Schrödinger equation (NLSE) [12]. To derive this equation, we choose a carrier frequency ω_0 which is close to the frequency of the pulse we are considering and consider its associated wave number via the linear dispersion relation of the medium or waveguide. At ω_0, the linear dispersion relation has a slope $\beta_1 \equiv d\beta/d\omega$, and a curvature $\beta_2 \equiv d^2\beta/d\omega^2$. Apart from a multiplying factor describing the transverse shape of the mode, the complex electric field of the pulse is written as $\psi(z, t)e^{-i\omega_0 t}$, where ψ is the envelope and t is time. It is then found that ψ satisfies

$$i\frac{\partial \psi}{\partial z} + i\beta_1 \frac{\partial \psi}{\partial t} - \frac{\beta_2}{2}\frac{\partial^2 \psi}{\partial t^2} + \gamma|\psi|^2\psi = 0, \quad (1)$$

where γ is the nonlinear parameter. The usual form of the NLSE is obtained using the coordinates

$$Z = z, \quad T = t - \beta_1 z, \quad (2)$$

where T is the retarded time. In these coordinates, a pulse propagating at the velocity $1/\beta_1$ is stationary. In terms of Z

and T, Eq. (1) takes the form

$$i\frac{\partial \psi}{\partial Z} - \frac{\beta_2}{2}\frac{\partial^2 \psi}{\partial T^2} + \gamma|\psi|^2\psi = 0, \quad (3)$$

which is the standard NLSE [13]. Equation (3) implies that we assumed the linear dispersion relation $\beta = \beta(\omega)$ to be a parabolic function so that higher-order derivatives are absent or negligible. This is generally true in standard optical waveguides at the central frequency ω_0 away from the zero-dispersion wavelength [13]. One implication is that if we change the reference frequency ω_0 then Eq. (3) is unchanged. This property, that the evolution equation is independent of the frame in which it applies, is referred to as *Galilean invariance*.

A consequence of Galilean invariance is that solutions of Eq. (1) do not depend on the speed at which they propagate. In particular, its fundamental soliton solutions, which require $\beta_2 < 0$, form a two-parameter family, with the first parameter (μ) determining the soliton's amplitude and energy, whereas the second parameter is the group velocity v with respect to the frame that is used to describe it. However, the latter can always be made to vanish by choosing an appropriate reference frame via Eq. (2). Solitons lacking Galilean invariance were earlier studied in the context of Bose-Einstein condensates [14–18].

Recent studies have demonstrated experimentally and numerically the existence of *pure-quartic solitons* (PQSs), which arise from the balance between self-phase modulation and negative fourth-order dispersion ($\beta_4 < 0$) [19–22]. They have different properties than conventional solitons, with potential applications in high-energy pulse lasers and microresonator frequency combs [21–23]. PQSs exist at a unique carrier frequency ω_0 where both the quadratic (β_2) and cubic (β_3) dispersion vanish. PQSs satisfy the modified NLSE [19,20]

$$i\frac{\partial \psi}{\partial Z} + \frac{\beta_4}{4!}\frac{\partial^4 \psi}{\partial T^4} + \gamma|\psi|^2\psi = 0, \quad (4)$$

*Corresponding author: martijn.desterke@sydney.edu.au

with $\beta_4 < 0$, and they propagate at the group velocity associated with the frequency ω_0. However, Eq. (4), in contrast to Eq. (3), is not Galilean invariant: changing the reference frequency ω_0 not only changes the group velocity but also leads to nonzero quadratic and cubic dispersion terms. Concretely, for a quartic dispersion relation centered at ω_0 and defined as $\beta(\omega) = \beta_4(\omega - \omega_0)^4/24$, a detuning Δ in the carrier frequency introduces quadratic and cubic dispersion terms, and Eq. (4) becomes

$$i\frac{\partial\psi}{\partial Z} - \Delta^2\frac{\beta_4}{4}\frac{\partial^2\psi}{\partial T^2} - i\Delta\frac{\beta_4}{6}\frac{\partial^3\psi}{\partial T^3} + \frac{\beta_4}{4!}\frac{\partial^4\psi}{\partial T^4} + \gamma|\psi|^2\psi = 0, \tag{5}$$

in the frame associated with the frequency $\omega_0 + \Delta$. Thus, changing frames leads to effective quadratic and cubic dispersions $\bar{\beta}_2 = \Delta^2\beta_4/2$ and $\bar{\beta}_3 = \Delta\beta_4$, respectively. The effects of this additional dispersion on the properties of PQSs have yet to be reported.

In this paper, we investigate theoretically and numerically the consequences of a lack of Galilean invariance of Eq. (4) for the PQS properties. We find that the resulting soliton pulses form a continuous family of solitons that can be parametrized by their amplitude and by their detuning Δ and that differ in shape from PQSs. Our results show that although the temporal power remains symmetric, for $\Delta \neq 0$ the phase is no longer constant and the spectrum becomes asymmetric. Using propagation simulations, we show that these soliton solutions are stable. These results provide insights on temporal solitons in the presence of higher-order dispersion and we expect them to stimulate future studies in other areas of physics and applied mathematics.

The outline of this paper is as follows. In Sec. II we investigate stationary solutions of Eq. (5) using two approaches. First, in Sec. II A we use an analytic approach that gives the properties of the solitons' tails. In Sec. II B we use a numerical approach to find full stationary solutions. We investigate the stability of these solutions using propagation simulations in Sec. III. The expression for the energy flow in the presence of high-order dispersion is discussed in Sec. IV. In Sec. V we briefly discuss the dynamics of these solutions in simulations of collisions. Finally, in Sec. VI we discuss our results and conclude.

II. STATIONARY SOLUTIONS

In this section we investigate stationary solutions of Eq. (5) using an ansatz of the form

$$\psi(Z, T) = u(T)e^{i\mu z} \tag{6}$$

so the shape is preserved during propagation. Function u thus satisfies

$$-\mu u - \Delta^2\frac{\beta_4}{4}\frac{\partial^2 u}{\partial T^2} - i\Delta\frac{\beta_4}{6}\frac{\partial^3 u}{\partial T^3} + \frac{\beta_4}{4!}\frac{\partial^4 u}{\partial T^4} + \gamma|u|^2 u = 0. \tag{7}$$

Although in the presence of quadratic dispersion u can be taken to be real, in the more general case considered here, this is not so.

We first consider the low-intensity limit of Eq. (7) in which the nonlinear term is neglected. This gives analytic results about the tails of the solutions [20,24]. We then solve

Eq. (7) numerically using the Newton-conjugate-gradient method [25,26] to find full stationary solutions. In all of our numerical calculations we take $\beta_4 = -2.2$ ps^4 mm^{-1}, $\mu = 1.76$ mm^{-1}, and $\gamma = 4.07$ W^{-1} mm^{-1}.

A. Linear limit–tail analysis

We consider the low-intensity limit in which the nonlinear term in Eq. (7) can be neglected. The resulting linear differential equation has solutions of the form

$$\sum_{j=1}^{4} a_j e^{\lambda_j T}, \tag{8}$$

where the a_j's are complex constants and the λ_j's satisfy the algebraic equation

$$\lambda^4 - 4i\Delta\lambda^3 - 6\Delta^2\lambda^2 + \frac{24\mu}{|\beta_4|} = 0, \tag{9}$$

where we have explicitly indicated that $\beta_4 < 0$. It is straightforward to see that, if λ is a solution, then so is $-\lambda^\star$. Therefore, the solutions are symmetric with respect to the imaginary axis, with the roots for which $\text{Re}(\lambda) > 0$, i.e., exponentially increasing with time, corresponding to the leading edge of the pulse, and similarly the roots with $\text{Re}(\lambda) < 0$ correspond to the trailing edge. As we see in Sec. II B, this symmetry is consistent with the finding that the power of the solutions is symmetric in time.

When $\Delta = 0$, Eq. (9) has the four solutions $\lambda = (6\mu/|\beta_4|)^{1/4}(\pm 1 \pm i) \equiv \eta(\pm 1 \pm i)$, forming a square in the complex plane [20]. This implies that the tails of the solitons are real and take the form $e^{\pm\eta T}\cos(\eta T + \phi)$, where ϕ is a phase that can only be found from solving the full nonlinear equation, and where the signs apply to the leading and the trailing edges.

For $\Delta \neq 0$, but sufficiently small so that the term in Δ^2 can be neglected, the roots are found to be $\lambda \approx \eta(\pm 1 \pm i) + i\Delta$. Thus the roots move vertically in the complex plane, reflecting the change in the reference frequency.

We determine the roots numerically when the linear and quadratic terms in Δ are comparable in magnitude. However, when Δ is sufficiently large so that the quadratic term in λ dominates the cubic and quartic terms, then we find that $\lambda = \pm\sqrt{4\mu/|\beta_4|}/\Delta$. Including the cubic term in Eq. (9) then gives the better approximation

$$\lambda = \pm\sqrt{\frac{4\mu}{|\beta_4|}}\frac{1}{\Delta}\left(1 \mp \frac{2}{3}i\sqrt{\frac{\mu}{|\beta_4|}}\frac{1}{\Delta^2}\right). \tag{10}$$

Substituting the result without the correction into Eq. (9), it is then found that the other two roots are approximately $\lambda = \sqrt{2}(\pm 1 + i\sqrt{2})\Delta$. The transition between the regime where Δ is small, in which the roots move vertically, and where Δ is sufficiently large to cause the solutions to change substantially can be estimated as the intersection of the approximate expressions for the positions of the roots. By setting the real part of Eq. (10) equal to η, we find the critical detuning

$$\Delta_c = \frac{2}{6^{1/4}}\left(\frac{\mu}{|\beta_4|}\right)^{1/4} \approx 1.28\left(\frac{\mu}{|\beta_4|}\right)^{1/4}. \tag{11}$$
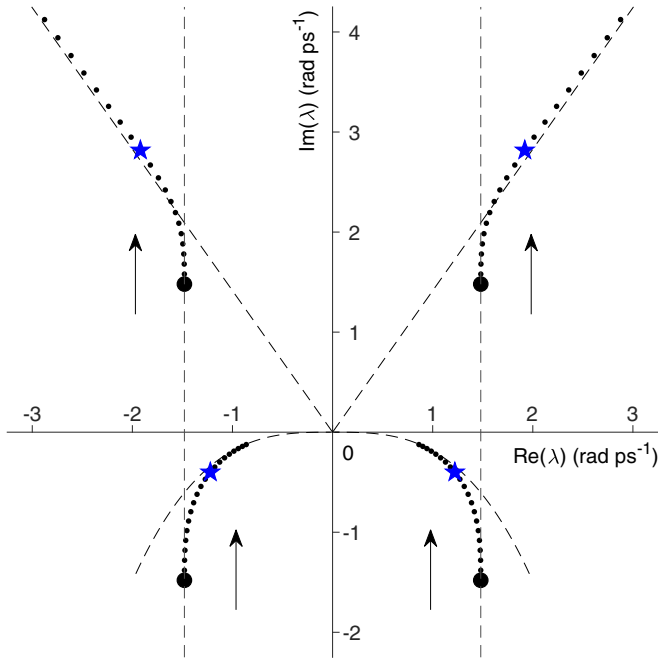
FIG. 1. Roots λ in the complex plane with Δ increasing from $\Delta = 0$ (large dots) to $\Delta = 2$ rad ps^{-1} in steps of 0.1 rad ps^{-1} in the directions of the arrows. The vertical dashed lines give the asymptotes as $\Delta \to 0$, whereas the diagonal dashed lines and the dashed curves are the asymptotes as $\Delta \to \infty$. The blue stars give the location of the roots when $\Delta = \Delta_c$.

A numerical calculation of the roots is shown in Fig. 1. For $\Delta = 0$, the roots form a square in the complex plane, indicated by the four large dots. As Δ increases, they move in a way consistent with the previous discussion, with two of them moving toward the origin and two moving to infinity. One may expect that the roots for which $|\text{Re}(\lambda)|$ is smallest to dominate, as they correspond to the lowest decay rate [20]. Hence, as Δ increases, the two roots moving to the origin become increasingly dominant. This reflects the fact that, far from the apex, a quartic curve locally approaches a parabola. When $\Delta < 0$, the root structure is identical as described here, but the roots move down rather than up.

B. Stationary solutions

In this section, we show numerical stationary solutions to Eq. (7). We use a Newton-conjugate-gradient method developed by Yang [26], which acts as an optimization method and converges to a solution if the initial guess is appropriate. This method is adapted for complex solutions based on Yang's code for computing complex eigenvalues of vortex solitons. The difficulty in determining these solutions is related to finding appropriate initial guesses and selecting appropriate accelerators for the numerical method [25]. For $\Delta \neq 0$, we use the (real) solution to the PQS for $\Delta = 0$ as the input guess [20]. We numerically solve Eq. (7) for three different values of detuning, Δ.

The numerical solutions for $\Delta = 0$, $\Delta = 0.75\Delta_c$, and $\Delta = 1.5\Delta_c$ are shown in the first, middle, and bottom rows of Fig. 2, respectively. The left column shows the temporal

power and phase profiles, while the middle column gives the corresponding spectrum. Finally, the right column shows the two-dimensional Fourier transform with respect to time and position [24]. For $\Delta = 0$, the solution is a PQS, similar to those obtained earlier, that we include for comparison. In particular, the temporal shape exhibits oscillating tails and associated π phase jumps, as seen in Fig. 2(a), while the spectrum is symmetric with a somewhat flattened peak, as seen in Fig. 2(b). Finally, the two-dimensional Fourier transform, shown in Fig. 2(c), forms a straight horizontal line with the colors indicating the amplitude following the curve in Fig. 2(b). We also provide the linear dispersion relation. The two-dimensional Fourier transform of the soliton and the linear dispersion relation are separated by μ and do not intersect, indicating that the soliton cannot radiate into linear waves [24].

Figures 2(d)–2(f) are similar to Figs. 2(a)–2(c), but for $\Delta = 0.75\Delta_c \approx 0.906$ rad ps^{-1} for our parameters. Figure 2(d) presents again the power versus time (blue curve). It shows that the oscillations in the tails have been substantially suppressed because the roots moving to the origin via the real axis are starting to dominate. The phase now exhibits a ramp associated with the vertical shift of the roots, though it retains remnants of the phase jumps shown in Fig. 2(a). The spectrum given in Fig. 2(e) is distinctly asymmetric. This can be understood by considering Fig. 2(f), showing the two-dimensional Fourier transform of the soliton superimposed on the linear dispersion relation. The latter is also asymmetric due to the frequency shift and the subsequent change of frame. As a consequence, high frequencies tend to be further away from the linear dispersion relation than low frequencies, and they, therefore, have a lower amplitude. This can also be understood as following from the presence of cubic dispersion.

The trends mentioned in the previous paragraph continue in Figs. 2(g), 2(h), and 2(i), giving the solution for $\Delta = 1.5\Delta_c \approx 1.813$ rad ps^{-1}. This is truly the asymptotic regime for which the quadratic dispersion is large. The power in Fig. 2(g) appears to have a hyperbolic secant shape and the phase profile exhibits an approximate linear ramp, with a modest feature in the center. This indicates that the quadratic dispersion is dominating, consistent with $\Delta > \Delta_c$. Although the spectrum is asymmetric, particularly down in the tails, it is less so than in Fig. 2(e). This is consistent with Fig. 2(i), which shows that the linear dispersion relation is approximately parabolic around the maximum and that the cubic dispersion, which causes the asymmetry, is only apparent for frequencies far from the maximum.

We now consider the energy $U = \int |u|^2 dT$ of these soliton solutions. Results of such calculations are shown in Fig. 3, in which the solid curve shows the energy versus the normalized detuning Δ/Δ_c. The top axis shows the associated inverse speed β_1. The fact that the soliton energy depends on the speed is consistent with the lack of Galilean invariance. More specifically, the figure shows that the pulse energy appears to vary slowly when $\Delta \lesssim \Delta_c$, but for $\Delta \gtrsim \Delta_c$, for which $\bar{\beta}_2$ dominates, it varies approximately linearly with Δ. This can be understood as follows. It is straightforward to ascertain that for a conventional, nonlinear Schrödinger soliton,
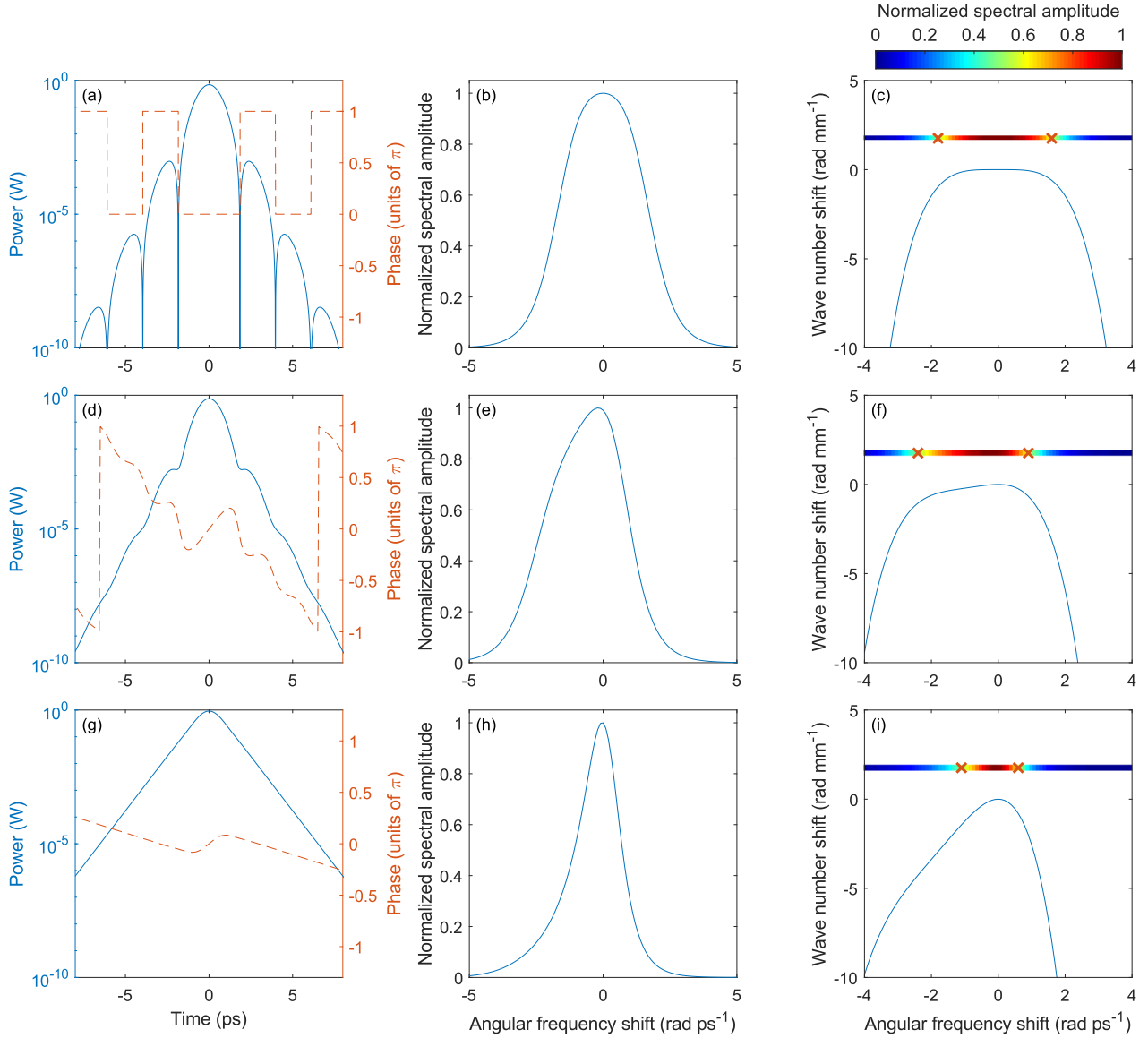
FIG. 2. Solutions to Eq. (7) for different values of Δ. The solution for $\Delta = 0$ rad ps^{-1} is given along the first row, showing (a) power (blue curve, logarithmic scale) and phase (orange dashed curve) versus time. (b) Normalized spectral amplitude. (c) Normalized two-dimensional Fourier transform in arbitrary units (see color bar), with the crosses indicating the full-width at half maximum. The linear dispersion relation about ω_0 is shown for comparison (blue curve). Analogous results are shown for $\Delta = 0.75\Delta_c \approx 0.906$ rad ps^{-1} in panels (d), (e), and (f) along the second row and $\Delta = 1.5\Delta_c \approx 1.813$ rad ps^{-1} in panels (g), (h), and (i) along the third row.

$U = \sqrt{8\mu|\beta_2|}/\gamma$. We discussed in Sec. I that here $\bar{\beta}_2 = \Delta^2\beta_4/2$. Combining this with the definition of Δ_c in Eq. (11), it is then found that

$$ U = \frac{4}{\gamma}\left(\frac{\mu^3|\beta_4|}{6}\right)^{1/4}\frac{\Delta}{\Delta_c}. \tag{12} $$

This asymptotic result, which is superimposed in Fig. 3, is in excellent agreement with the full calculations.

Having illustrated that Eq. (4) has no Galilean invariance, we have shown that there exists a continuous set of solutions for every detuning Δ. Although we give results for a single value of μ, similar solutions exist for other values of this parameter. However, finding solutions to Eq. (7) does

not guarantee their stability—this can only be established by considering Eq. (5) which describes how the solutions evolve upon propagation. We turn to this next.

III. STABILITY OF THE SOLUTIONS

Establishing the stability of a nonlinear solution can be carried out using a formal stability analysis [20,25,27]. Perhaps a more direct way is to use the solutions from Sec. II B as an initial condition and then solve the evolution equation (5). This provides an excellent indication of stability, particularly when noise is added to the initial condition. This is the approach we take here. We consider $\Delta = 0.75\Delta_c$ in the most detail since the stability for $\Delta = 0$ was established earlier [20], whereas
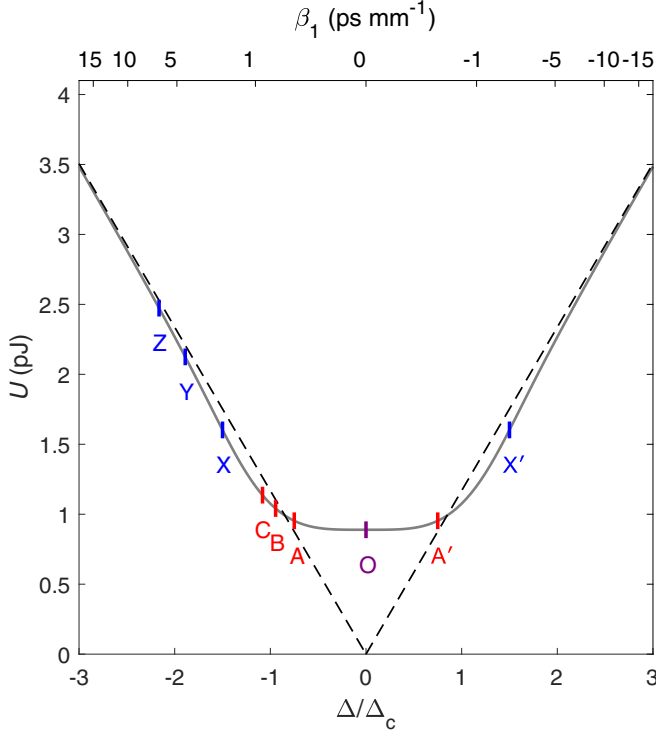
FIG. 3. Soliton energy versus normalized detuning Δ/Δ_c for a nonlinear system with pure-quartic dispersion, and $\mu = 1.76$ mm^{-1} in their stationary frames. Top axis gives the associated inverse group velocity β_1 in the frame where the dispersion is purely quartic. Dashed lines give the asymptotic result in Eq. (12). The labels refer to numerical experiments discussed in Sec. V.

for $\Delta = 1.5\Delta_c$ the pulse is close to a nonlinear Schrödinger soliton, the stability of which follows from the integrability of the governing equation.

Using the results from Sec. II B as initial conditions, we propagated for a distance of 100 L_4, where L_4 is the quartic dispersion length, the length scale over which the dispersion is expected to operate, which we define as [20]

$$L_4 = \frac{T_0^4}{|\beta_4|}, \tag{13}$$

where T_0 is the pulse's full width at half-maximum. For the detuning $\Delta = 0.75\Delta_c$, we have $T_0 = 1.192$ ps, so $L_4 = 0.916$ mm. For all cases, the pulse propagates without obvious changes to the profile. We then added 0.5% complex Gaussian noise to the solution, and the result is shown in Fig. 4 for the solution with $\Delta = 0.75\Delta_c$. Again there are no obvious dynamics as the pulse propagates, implying that it is stable. Carrying out a similar calculation for the solution with $\Delta = 1.5\Delta_c$ gives similar results. We have occasionally found that the soliton has a small residual speed. We attribute this to a small amount of momentum in the initial condition as a consequence of the inclusion of the noise.

IV. ENERGY FLOW

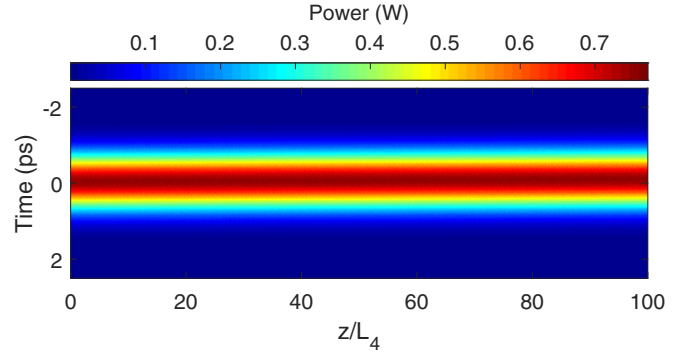The fundamental soliton solutions to the NLSE can be made real since they have a uniform phase. This reflects the

FIG. 4. Propagation simulation with 0.5% complex Gaussian noise for the solution with $\Delta = 0.75\Delta_c \approx 0.906$ rad ps^{-1} using the split-step Fourier method with spatial step size $\Delta z = 0.5$ μm over 100 L_4.

absence of an energy flow within the soliton—if this energy flow was nonzero, then the energy would deplete at some positions and increase elsewhere, which is inconsistent with stationary $e^{i\mu z}$ dependence. Pure-quartic solitons can also be made real, albeit with changes in sign, for the same reason. In contrast, the solitons with $\Delta \neq 0$ we discussed in Sec. II B do not have this property. This is particularly evident in Fig. 2(d), which shows a highly nonuniform phase φ with an associated nonuniform instantaneous frequency of $-\partial\varphi/\partial T$. We now set out to understand this.

We derive an expression for the energy flow in the presence of quadratic, cubic, and quartic dispersion. Our starting point is the expression for energy conservation with one spatial dimension:

$$\frac{\partial J}{\partial T} = -\frac{\partial(\psi^\star\psi)}{\partial Z}, \tag{14}$$

where $\rho = \psi^\star\psi$ is the energy density and J is the energy flow, the expression for which we aim to find. We note that this expression differs from the usual conservation laws, since in Eq. (5), Z is the evolution parameter, rather than T. Even though J, therefore, does not have the units of an energy flow [J m^{-1} (m s^{-1})$^{-1}$ rather than J s^{-1} = J m^{-1} (m s^{-1})], it is a related quantity and we will, therefore, refer to it as the "energy flow."

We now use the evolution equation (5) to evaluate the right-hand side of Eq. (14), and then we write it as a time derivative as on the left-hand side of Eq. (14). In doing this we consider the general case with general $\beta_{3,4}$, rather than the expressions involving Δ that arise in the specific problem considered here, and we include β_1 for completeness. This calculation can be done dispersion order-by-dispersion order. To illustrate this, for quadratic dispersion, it is found that

$$\psi_{TT} = [u'' + i(2u'\varphi' + u\varphi'') - u(\varphi')^2]e^{i\varphi}, \tag{15}$$

where the prime (') indicates a time derivative and ψ is written as $\psi = ue^{i\varphi}$. We, therefore, find

$$\psi^\star\psi_{TT} - \psi\psi_{TT}^\star = 2i(2uu'\varphi' + u^2\varphi'') = 2i(u^2\varphi')'. \tag{16}$$

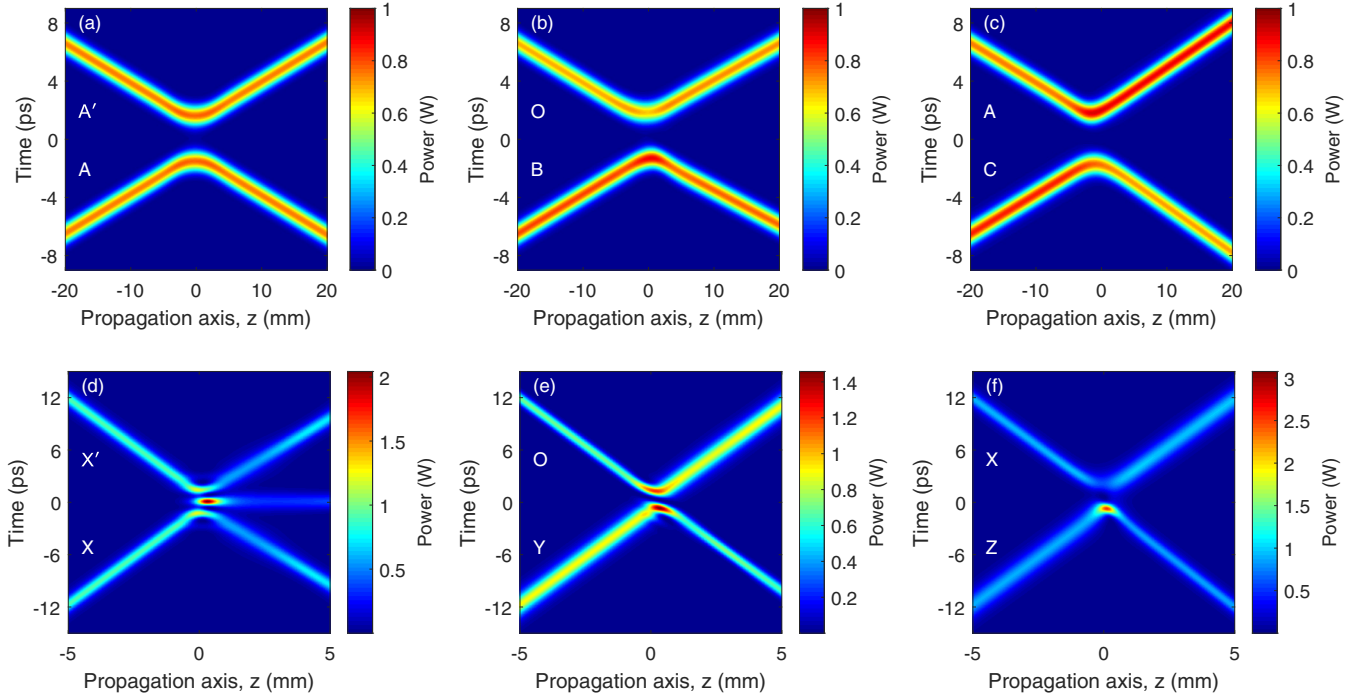Thus following Eq. (5), the energy flow associated with quadratic dispersion is $-\beta_2 u^2\varphi'$. Applying the same

FIG. 5. Collisions of solitons with different values of Δ of the same family generated by $\mu = 1.76$ mm^{-1}. The initial conditions are as follows: (a) $\Delta\beta_1 = \Delta\beta_1^{(a)}$, $\langle\beta_1\rangle = 0$; (b) $\Delta\beta_1 = \Delta\beta_1^{(a)}$, $\langle\beta_1\rangle = \Delta\beta_1^{(a)}$; (c) $\Delta\beta_1 = \Delta\beta_1^{(a)}$, $\langle\beta_1\rangle = 2\Delta\beta_1^{(a)}$; (d) $\Delta\beta_1 = \Delta\beta_1^{(b)}$, $\langle\beta_1\rangle = 0$; (e) $\Delta\beta_1 = \Delta\beta_1^{(b)}$, $\langle\beta_1\rangle = \Delta\beta_1^{(b)}$; and (f) $\Delta\beta_1 = \Delta\beta_1^{(b)}$, $\langle\beta_1\rangle = 2\Delta\beta_1^{(b)}$. Each collision is shown in the frame of reference which moves at this average inverse velocity. Text labels indicate the solitons in Fig. 3.

procedure to the other dispersion orders, we find

$$J = \beta_1 u^2 - \beta_2 u^2 \varphi' - \frac{\beta_3}{6}[2uu'' - (u')^2 - 3u^2(\varphi')^2]$$
$$+ \frac{\beta_4}{12}[4uu''\varphi' + 2uu'\varphi'' + u^2\varphi''' - 2(u')^2\varphi' - 2u^2(\varphi')^3].$$
(17)

The β_1 term expresses that in the absence of dispersion, a pulse propagates as a rigid object with energy u^2 propagating at inverse group velocity β_1. The β_2 term shows that when φ is constant, then the energy flow vanishes, consistent with the discussion in the first paragraph of this section, and a similar conclusion applies to the β_4 term. The β_3 term is different in that $\varphi' = 0$ does not guarantee that the energy flow vanishes, because of the presence of the $2uu'' - (u')^2$ terms. This confirms that in the presence of cubic dispersion, stationary solutions cannot have a constant phase. We explicitly evaluated the energy flow for the soliton in Fig. 2(d) and have confirmed that the energy flow is constant, even though the phase has a complicated time dependence.

V. COLLISION DYNAMICS

In the frame with only $\beta_4 \neq 0$, the solutions from Sec. II have a constant inverse velocity of $\bar{\beta}_1 = -\Delta^3\beta_4/6$. Having shown their stability and lack of Galilean invariance, we investigate collisions between these pulses using a fourth-order propagation method [25]. However, the energy U dependence on v (see Fig. 3) adds a complication. To ensure collisions between comparable solitons, we can choose to keep either

μ or U the same but not both. In these collisions, we keep $\mu = 1.76$ mm^{-1} constant for all initial solitons, implying that the nonlinear effects they induce are roughly constant. We carry out our simulations as before, but with a propagation step size of $\Delta z = 0.25$ μm.

We find a wide variety of dynamical results when varying both the relative speeds of the pulses and their average speeds with respect to the pure-quartic frame. We present in Fig. 5 some representative collisions for pairs of solitons with the same relative inverse velocities at $\Delta\beta_1^{(a)} \equiv |2(0.75\Delta_c)^3\beta_4/6| \approx 0.546$ ps mm^{-1} (top row) and $\Delta\beta_1^{(b)} \equiv |2(1.5\Delta_c)^3\beta_4/6| \approx 4.369$ ps mm^{-1} (bottom row), but with different average inverse velocities with respect to the pure-quartic frames of $\langle\beta_1\rangle = 0$, $\Delta\beta_1^{(a,b)}$, and $2\Delta\beta_1^{(a,b)}$ for the left, center, and right columns, respectively. Note that $\Delta\beta_1^{(a)}$ is chosen such that, when $\langle\beta_1\rangle = 0$, the colliding solitons are the solution observed in Fig. 2(d), with one having the opposite phase. The same is true for $\Delta\beta_1^{(b)}$ but referring to Fig. 2(g).

For convenience, each simulated collision has been transformed to the frame of reference which moves at their average inverse velocity, $\langle\beta_1\rangle$. A summary of each collision shown is detailed in Table I featuring numerically calculated inverse velocities in this frame and peak powers for the solitons which enter and exit the collision.

Figure 5(a) shows a collision between two solitons with equal speeds $|\beta_1^{(a)}|$ propagating in opposite directions, generated by the detuning $|\Delta| = 0.75\Delta_c$. Labeled as points A and A' in Fig. 3, these pulses have the same energy, so the initial condition is symmetric about $T = 0$. Likewise, the exiting solitons are found to be symmetric about $T = 0$, but each

TABLE I. Properties of entering and exiting solitons in the collisions in Fig. 5. Relative inverse velocities between initial solitons ($\Delta\beta_1$) and average inverse velocity of initial solitons with respect to the pure-quartic dispersion frame ($\langle\beta_1\rangle$) are given. The inverse velocities with respect to the average inverse velocity and peak powers for the top pulse localized to $T > 0$ are given by $\beta_1^{(+)}$ and $P_{\text{peak}}^{(+)}$, and, similarly, for the bottom pulse localized to $T < 0$ they are given by $\beta_1^{(-)}$ and $P_{\text{peak}}^{(-)}$.

			Entering solitons				Exiting solitons			
Panel	$\Delta\beta_1$ (ps mm^{-1})	$\langle\beta_1\rangle$ (ps mm^{-1})	$\beta_1^{(+)}$ (ps mm^{-1})	$P_{\text{peak}}^{(+)}$ (W)	$\beta_1^{(-)}$ (ps mm^{-1})	$P_{\text{peak}}^{(-)}$ (W)	$\beta_1^{(+)}$ (ps mm^{-1})	$P_{\text{peak}}^{(+)}$ (W)	$\beta_1^{(-)}$ (ps mm^{-1})	$P_{\text{peak}}^{(-)}$ (W)
(a)	0.5461	0	−0.2731	0.7496	0.2731	0.7496	0.2729	0.7492	−0.2729	0.7492
(b)	0.5461	0.5641	−0.2731	0.6972	0.2731	0.8022	0.2522	0.7294	−0.2396	0.7690
(c)	0.5461	1.0922	−0.2731	0.7496	0.2731	0.8438	0.3080	0.8828	−0.3165	0.7100
(d)	4.3689	0	−2.1844	0.9147	2.1844	0.9147	1.8018	0.6891	−1.8018	0.6891
(e)	4.3689	4.3689	−2.1844	0.6972	2.1844	0.8953	2.1368	0.8421	−2.1449	0.6739
(f)	4.3689	8.7377	−2.1844	0.9147	2.1844	0.8827	2.1518	0.9711	−2.3336	0.8576

pulse has slowed marginally (Table I) with the generation of small amounts of radiation.

Figure 5(b) shows a stationary PQS colliding with a soliton with an inverse velocity of $\beta_1 = 2|\beta_1^{(a)}|$. Labeled O and B in Fig. 3, the pulse energies are different and the initial condition is asymmetric about $T = 0$. Likewise, the exiting solitons are also asymmetric, with the top exiting pulse retaining a peak power lower than that of the bottom exiting pulse, similar to the initial solitons. Both exiting pulses appear to have a lower inverse velocity, but to different degrees (see Table I).

Figure 5(c) is similar, but the solitons have initial inverse speeds $\beta_1 = |\beta_1^{(a)}|$ and $\beta_1 = 3|\beta_1^{(a)}|$, and thus they have the same sign. These pulses have substantially different energies (see points A and C in Fig. 3), which, as in Fig. 5(b), is reflected in the asymmetry of the collision products. However, in contrast to the earlier result, the inverse speeds of the exiting solitons are now higher in the average inverse velocity frame, and relative peak powers of the collision products are reversed compared to Fig. 5(b).

For the collisions in Figs. 5(d), 5(e), and 5(f), the moving solitons have $|\Delta| > \Delta_c$. These collisions also demonstrate obvious changes in dynamics as $\langle\beta_1\rangle$ is changed. This is most clear where Fig. 5(d) with a symmetric initial condition produces a third pulse with $\beta_1 = 0$ and non-negligible peak power, while in Fig. 5(e), which is initially asymmetric, this is not so. Meanwhile, close examination of the collision in Fig. 5(f) indicates the presence of an extremely weak third pulse with only ∼1/500 the peak power of the other exiting solitons. We note that a change in the number of solitons in a collision in a geometry lacking Galilean invariance was observed previously [15].

The results in the table show that, whereas in most collisions the peak power and the inverse speeds do not change significantly, substantial changes can occur when the collisions are made more asymmetric. These tabulated results further indicate that, in most collisions, the soliton which initially has the higher (lower) peak power has its peak power reduced (raised) following the collision, though we find no clear trend describing the extent to which this occurs. One exception where this is not observed is for the collision in Fig. 5(f). There is also no clear trend in the changes of β_1 in these collisions.

VI. DISCUSSION AND CONCLUSION

We have shown that the generalized NLSE with pure-quartic dispersion does not have Galilean invariance, and we have illustrated this by demonstrating that the solutions depend on their speed. This is distinct from earlier works showing the lack of Galilean invariance due to spin-orbit coupling in spinor Bose-Einstein condensates [14–18]. We find numerically that the power of the solutions is symmetric in time, consistent with an analysis of the tails. We also find that the solutions have an asymmetric spectrum, which can be understood from the asymmetry of the linear dispersion relation. Based on propagation simulations, with and without noise, we conclude that these solutions are likely to be stable. Although these solitons have a complicated phase, the associated energy flow is constant. Simulating collisions between pairs of solutions generates a plethora of different dynamics depending on their relative speeds and average speeds with respect to the pure-quartic frame. The unusual dynamics indicate further consequences of the lack of Galilean invariance.

While the existence of soliton solutions to Eq. (7) at different speeds may not be surprising, it is perhaps not obvious that such pulses are stable. The effect of higher-order dispersion on single solitons with dominant quadratic dispersion has been extensively analyzed [8,9,28–30] with the conclusion that the pulse distorts strongly and that a substantial part of the energy transfers to linear waves and disperses [28]. However, it has been shown that the inclusion of quartic dispersion stabilizes the pulses [31], which is consistent with the results obtained here. While we did not prove stability conclusively, we believe that our numerical results are convincing without the need for more rigorous methods. We note that to our knowledge the validity of the Vakhitov-Kolokolov stability criterion [1] has not been established for soliton solutions of Eq. (5).

We did not discuss the effects of phase differences between the colliding initial solitons in Sec. V. However, we found that this phase strongly affects the collision (as it does for conventional solitons). For example, introducing a π phase difference between the initial solitons in Fig. 5(d) prevents the third central pulse from forming.

The overarching conclusion is that for a given dispersion relation, PQSs only exist at the frequency for which $\beta_2 = 0$ and $\beta_3 = 0$ (if such a frequency exists), and they

travel at the group velocity at this frequency. Solutions of the type discussed here occur at other frequencies, and they evolve towards conventional nonlinear Schrödinger solitons at large detunings. Of course, in systems with a programmable dispersion [22,23], PQSs can exist for a range of frequencies.

ACKNOWLEDGMENTS

[1] Y. S. Kivshar and G. P. Agrawal, *Optical Solitons: From Fibers to Photonic Crystals*, 1st ed. (Elsevier Science, Amsterdam, 2003).

[2] L. F. Mollenauer, M. J. Neubelt, M. Haner, E. Lichtman, S. G. Evangelides, and B. M. Nyman, Electron. Lett. **27**, 2055 (1991).

[3] H. A. Haus and W. S. Wong, Rev. Mod. Phys. **68**, 423 (1996).

[4] L. F. Mollenauer and R. H. Stolen, Opt. Lett. **9**, 13 (1984).

[5] F. Leo, S. Coen, P. Kockaert, S.-P. Gorza, P. Emplit, and M. Haelterman, Nat. Photonics **4**, 471 (2010).

[6] T. Herr, V. Brasch, J. D. Jost, C. Y. Wang, N. M. Kondratiev, M. L. Gorodetsky, and T. J. Kippenberg, Nat. Photonics **8**, 145 (2014).

[7] T. J. Kippenberg, A. L. Gaeta, M. Lipson, and M. L. Gorodetsky, Science **361**, eaan8083 (2018).

[8] J. N. Elgin, Opt. Lett. **17**, 1409 (1992).

[9] Y. Kodama, M. Romagnoli, S. Wabnitz, and M. Midrio, Opt. Lett. **19**, 165 (1994).

[10] A. Höök and M. Karlsson, Opt. Lett. **18**, 1388 (1993).

[11] I. P. Christov, M. M. Murnane, H. C. Kapteyn, J. Zhou, and C.-P. Huang, Opt. Lett. **19**, 1465 (1994).

[12] V. E. Zakharov and A. B. Shabat, Sov. Phys. JETP **34**, 62 (1972).

[13] G. P. Agrawal, *Nonlinear Fiber Optics*, 2nd ed. (Academic Press, San Diego, 1995).

[14] Y. Xu, Y. Zhang, and C. Zhang, Phys. Rev. A **92**, 013633 (2015).

[15] H. Sakaguchi, B. Li, and B. A. Malomed, Phys. Rev. E **89**, 032920 (2014).

[16] A. Tononi, Y. Wang, and L. Salasnich, Phys. Rev. A **99**, 063618 (2019).

[17] Z. Fan, Z. Chen, Y. Li, and B. A. Malomed, Phys. Rev. A **101**, 013607 (2020).

[18] G. A. Sekh and B. Talukdar, Phys. Lett. A **415**, 127665 (2021).

[19] A. Blanco-Redondo, C. M. de Sterke, J. E. Sipe, T. F. Krauss, B. J. Eggleton, and C. Husko, Nat. Commun. **7**, 10427 (2016).

[20] K. K. K. Tam, T. J. Alexander, A. Blanco-Redondo, and C. M. de Sterke, Opt. Lett. **44**, 3306 (2019).

[21] H. Taheri and A. B. Matsko, Opt. Lett. **44**, 3086 (2019).

[22] A. F. J. Runge, D. D. Hudson, K. K. K. Tam, C. M. de Sterke, and A. Blanco-Redondo, Nat. Photonics **14**, 492 (2020).

[23] A. F. J. Runge, Y. L. Qiang, T. J. Alexander, M. Z. Rafat, D. D. Hudson, A. Blanco-Redondo, and C. M. de Sterke, Phys. Rev. Research **3**, 013166 (2021).

[24] N. Akhmediev and M. Karlsson, Phys. Rev. A **51**, 2602 (1995).

[25] J. Yang, *Nonlinear Waves in Integrable and Nonintegrable Systems*, 1st ed. (SIAM, Philadelphia, 2010).

[26] J. Yang, J. Comput. Phys. **228**, 7007 (2009).

[27] D. E. Pelinovsky, Y. S. Kivshar, and V. V. Afanasjev, Physica D (Amsterdam, Neth.) **116**, 121 (1998).

[28] G. P. Agrawal and M. J. Potasek, Phys. Rev. A **33**, 1765 (1986).

[29] J. Elgin, T. Brabec, and S. Kelly, Opt. Commun. **114**, 321 (1995).

[30] S. Roy, S. K. Bhadra, and G. P. Agrawal, Phys. Rev. A **79**, 023824 (2009).

[31] M. Piché, J.-F. Cormier, and X. Zhu, Opt. Lett. **21**, 845 (1996).